remote sensing

Communication

Tropical Tropopause Layer Cloud Properties from Spaceborne Active Observations

Siliang Lei [1], Xijuan Zhu [2], Yuxiang Ling [1], Shiwen Teng [3] and Bin Yao [4,*]

[1] Collaborative Innovation Center on Forecast and Evaluation of Meteorological Disasters/China Meteorological Administration Aerosol-Cloud-Precipitation Key Laboratory, School of Atmospheric Physics, Nanjing University of Information Science & Technology, Nanjing 210044, China
[2] Science and Technology on Optical Radiation Laboratory, Beijing 100854, China
[3] College of Oceanic and Atmospheric Sciences, Ocean University of China, Qingdao 266100, China
[4] Key Laboratory of Transportation Meteorology of China Meteorological Administration, Nanjing Joint Institute for Atmospheric Sciences, Nanjing 210041, China
* Correspondence: yaobin@cma.gov.cn

Abstract: A significant part of clouds in the tropics appears over the tropopause due to intense convections and in situ condensation activity. These tropical tropopause layer (TTL) clouds not only play an important role in the radiation budget over the tropics, but also in water vapor and other chemical material transport from the troposphere to the stratosphere. This study quantifies and analyzes the properties of TTL clouds based on spaceborne active observations, which provide one of the most reliable sources of information on cloud vertical distributions. We use four years (2007–2010) of observations from the joint Cloud-Aerosol Lidar and Infrared Pathfinder Satellite Observations (CALIPSO) and CloudSat and consider all cloudy pixels with top height above the tropopause as TTL clouds. The occurrence frequency of TTL clouds during the nighttime is found to be almost 13% and can reach ~50–60% in areas with frequent convections. The annual averages of tropical tropopause height, tropopause temperature, and cloud top height are 16.2 km, −80.7 °C, and 16.6 km, respectively, and the average cloud top exceeds tropopause by approximately 500 m. More importantly, the presence of TTL clouds causes tropopause temperature to be ~3–4 °C colder than in the all-sky condition. It also lifts the tropopause heights ~160 m during the nighttime and lowers the heights ~84 m during the daytime. From a cloud type aspect, ~91% and ~4% of the TTL clouds are high clouds and altostratus, and only ~5% of them are associated with convections (i.e., nimbostratus and deep convective clouds). Approximately 30% of the TTL clouds are single-layer clouds, and multi-layer clouds are dominated by those with 2–3 separated layers.

Keywords: tropical tropopause layer; cloud property; satellite observation

Citation: Lei, S.; Zhu, X.; Ling, Y.; Teng, S.; Yao, B. Tropical Tropopause Layer Cloud Properties from Spaceborne Active Observations. *Remote Sens.* **2023**, *15*, 1223. https://doi.org/10.3390/rs15051223

Academic Editor: Itamar Lensky

Received: 10 January 2023
Revised: 20 February 2023
Accepted: 20 February 2023
Published: 22 February 2023

1. Introduction

The interface from the upper troposphere to the lower stratosphere is a transition layer rather than a material surface, and this region in the tropics is termed the tropical tropopause layer (TTL). The TTL normally ranges between approximately 14 km and 18.5 km and has physical and chemical characteristics midway between the upper troposphere and lower stratosphere [1,2]. Since upwelling air enters the stratosphere preferentially through the layer, the TTL exerts important controls in the stratospheric composition and global climate [1–3].

Although with little water vapor and high altitudes, there are still considerable clouds within and above TTL, especially occurring in the Western Pacific, South America, and Central Africa [4]. TTL clouds mainly contain widespread cirrus and those associated with convections, i.e., deep convective clouds as well as corresponding horizontally extended anvil clouds [1]. TTL convective clouds lift the water vapor and chemical species to the stratosphere, and TTL cirrus clouds accelerate the upwelling by enhanced radiation heating [5]. Moreover, through the greenhouse and albedo effects as well as the aforementioned gas transport [6], TTL clouds also have an influence on Earth's climate.

TTL cirrus clouds, optically thin clouds located around tropopause, may occur as frequently as 20 to 50% of the observation time [7,8]. They are predominantly composed of ice crystal particles [9] and are with physical thickness mostly less than one kilometer but spread hundreds of kilometers horizontally [10,11]. Meanwhile, the occurrence of deep convections and corresponding clouds decreases exponentially with increasing altitude in the tropopause region, and only approximately 0.5% of the clouds penetrate local tropopause in the tropics, and convection rarely penetrates the tropopause by more than 1.5 km [12]. Based on five years of Tropical Rainfall Measuring Mission data, Liu and Zipser [13] found that 1.3% of tropical convective systems surpass the 14 km level and 0.1% of them surpass approximately the 17 km level. Earth's radiation budget and climate depend on cloud radiative and geometric properties. Due to the vital role of TTL clouds, their characteristics are crucial for improving climate models and our understanding of TTL. However, better characterization of TTL cloud properties is challenging.

The most direct measurements come from an instrumented aircraft that penetrates convective clouds [14,15]. However, operational costs and safety concerns place severe constraints on flights for TTL clouds. Ground-based measurements (radiosonde, lidar, radar, etc.) are also suitable for investigating the detailed characteristics of cirrus clouds over a given location with high vertical and temporal resolutions. Pandit et al. [16] used collocated ground-based lidar and radiosonde measurements to study the characteristics of TTL cirrus clouds and their relationship with TTL. Hollars et al. [17] compared retrievals of cloud top heights (CTHs) based on ground-based millimeter-wave cloud radar measurements, and those from satellites, and found that results from radar agree well with those from satellite for thick clouds but are lower by as much as 2 km, and radar retrievals significantly underestimate CTHs of deep convective clouds. Similar to the limitations of aircraft measurements, ground-based instruments are also restricted by locations and cannot provide a wide range of observations.

Satellites are widely used in cloud detection because of their advantages of being free from geographical restrictions and all-weather detection. Passive satellite observation tends to detect cloud-top information [18]. Sherwood et al. [19] found that CTH obtained from thermal imagery suffers from a systematic low bias, and the highest part of the convective clouds is missed due to the relatively low spatial resolution. Active instruments (i.e., spaceborne lidar and radar) onboard satellites can better infer the vertical structures of clouds. A combination of collocated observations from spaceborne lidar and radar is clearly more advantageous in retrieving the three-dimensional structure of clouds than that from either lidar or radar. This is also possible due to the state-of-the-art A-Train collection [20], and joint observations from lidar onboard Cloud-Aerosol Lidar and Infrared Pathfinder Satellite Observations (CALIPSO) and from radar onboard CloudSat are commonly used in cloud researches. Sassen et al. [21] combined CALIPSO and CloudSat measurements to study tropical cirrus and deep convective clouds. Feng and Huang [22] adopt observations from joint CALIPSO and CloudSat to investigate the impacts of tropical cyclones on the thermodynamic conditions in TTL. However, research on TTL cloud properties is not yet mature, as most of the studies have been conducted separately for tropical cirrus clouds and convection, lacking overall studies of total TTL clouds. Moreover, TTL clouds are usually identified by a fixed TTL bottom [23] or by levels between the top of the convection and tropopause [24]. Those definitions of tropopause are not suitable for studying the properties of total TTL clouds.

To understand the qualitative and quantitative effect of TTL clouds on the tropopause and their role in the TTL process, long-term observations of TTL clouds are essential. This study uses joint active CALIPSO lidar and CloudSat radar observations to reveal the properties of total TTL clouds and the clouds are defined as pixels with top surpass tropopause. The data and method used are described in Section 2. TTL cloud macrophysical properties, e.g., CTH, cloud base height (CBH), cloud geometrical thickness (CGT), number of layers, classification, and phase, are presented and discussed in Sections 3 and 4. Section 5 concludes our work.

2. Data and Method

As parts of the A-Train satellite constellation, CloudSat and CALIPSO fly in the same orbit and with a close formation [20,25] providing near-simultaneous observations. These two active instruments detect targets in the microwave and visible and near-infrared bands, respectively, and can retrieve reliably atmospheric vertical structures from space. CloudSat carries a 94 GHz Cloud Profiling Radar (CPR) [20], and Cloud-Aerosol Lidar with Orthogonal Polarization (CALIOP) onboard CALIPSO is a nadir-viewing two-wavelength (532 nm and 1064 nm) polarization-sensitive lidar [25]. The vertical resolutions of CALIOP are 60 m and 180 m below and above 20.2 km altitude, respectively. The CPR gives oversampled profiles with a vertical resolution of 240 m. Radar signals are sensitive to large particles but are less sensitive to optically thin clouds, whereas lidar signals are sensitive to optically thin clouds but are rapidly attenuated in optically thick clouds. Therefore, their combination can provide one of the most reliable pictures of vertical structures and microphysical properties of clouds and aerosols.

As aforementioned, the height of the TTL base is typically defined as approximately 14.5 km and the height of the TTL top is approximately 18 km. Previous studies used average tropopause height (TH) as a threshold to classify TTL clouds, for example, Tseng and Fu [23] used a TTL base of 14.5 km to study TTL cirrus clouds. Such simple thresholds may cause an underestimation or overestimation of TTL clouds because tropopause itself varies with latitude, geographic location, season, etc. [4]. The fixed tropopause is inappropriate for our investigation of the total TTL clouds. Therefore, the tropopause information, including TH from Global Modeling and Assimilation Office Goddard Earth Observing System Model version 5 (GOES-5), is used as a feasible threshold, and the cloud pixels above the TH are considered as TTL clouds. Compare with previous research, the definition and method used in this study are more exact and reliable.

To facilitate the use of data, the CALIPSO team has integrated and stored the tropopause information of GOES-5 into the official CALIPSO product [26]. Therefore, we choose CALIPSO Level 2 version 4.20 5 km cloud profile product (05kmCPro) embedded with tropopause information [27]. The tropopause definition of GOES-5 is based on that of the typical lapse rate tropopause [23], which is defined as the lowest level at which the lapse rate ($-\mathrm{d}T/\mathrm{d}z$) drops under 2 °C/km. In this study, GOES-5 TH is used to define the location of the tropopause and further extract TTL clouds.

This study considers a combination of CALIOP and CPR observations, i.e., 2B-CLDCLASS-LIDAR version R05 product [28], to better infer TTL clouds including both optically thick clouds (i.e., deep convective clouds) and optically thin cirrus clouds. Compared with the original cloud classification product from either CloudSat or CALIPSO, the 2B-CLDCLASS-LIDAR can better detect complete cloud vertical structure to improve overall cloud detection and provide more reliable cloud type information. The 2B-CLDCLASS-LIDAR classifies clouds into high (cirrus and cirrostratus) clouds, altostratus (As), altocumulus (Ac), stratus (St), stratocumulus (Sc), cumulus (Cu), nimbostratus (Ns), and deep convective (cumulonimbus) clouds. The 2B-CLDCLASS-LIDAR product can also provide high-precision cloud vertical distributions, i.e., CTH and CBH in each layer and their corresponding phase information.

Studies have shown that the signal-to-noise ratio decreases during the daytime due to solar background noise [29]. However, due to a battery supply problem, CloudSat cannot collect detection measurements during the nighttime after 2011. To better compare the diurnal difference of TTL clouds and considering the observation limitation, we only collect continuous measurements from 2007 to 2010 of joint CALIPSO–CloudSat, and regions with latitudes between 30°S and 30°N are analyzed.

We perform the spatiotemporal collocation between 2B-CLDCLASS-LIDAR and 05km-CPro products to obtain the all-sky property dataset. According to the aforementioned definition, the TTL clouds and the corresponding cloud property, including TH and TT, CTH, CBH, cloud classification, and cloud phase in each profile, are extracted. In this study, TTL cloud pixels are within the uppermost cloud layer of each profile identified by the joint CloudSat–CALIPSO classification algorithm. Based on the layer identified by the 2B-CLDCLASS-LIDAR algorithm, we divide total TTL clouds into single-layer, multi-layer, and total TTL clouds. The number of total pixels are almost 50 million and approximately 9.2% of them (5 million) are TTL clouds.

3. Results

Spatial distributions of the seasonal TTL cloud fractions are shown in Figure 1, and both daytime (left panels) and nighttime (right panels) results are illustrated. The fraction is defined as the ratio between TTL cloud pixels and total observed pixels. The TTL cloud fraction is significantly lower during the daytime than that during the nighttime. During the nighttime, the average cloud fraction in the study area is about 13%, whereas the value halves to about 5% during the daytime. TTL cloud pixels detected during the nighttime and daytime are approximately 3.2 million and 1.3 million, respectively, indicating that the observation during the nighttime is approximately 2.5 times. This suggests that TTL clouds observed during the daytime are sparser than those during the nighttime. The diurnal discrepancy of cloud occurrence is also observed in previous studies for lidar detection. For example, Sassen et al. [28] used CALIPSO lidar observations to study the global distribution of cirrus clouds, which shows an approximately 10% diurnal variation in the tropics. It is consistent with our result that the average occurrence of high cloud (cirrus and cirrostratus) is 12% during the nighttime and that during the daytime is 4.7%, which is a 7.5% diurnal discrepancy. Although the detection efficiency of high clouds during the nighttime is higher for CALIOP due to the lower signal-to-noise ratio caused by solar background noise during the daytime [29], such instrumental and retrieval bias may result in a global loss of ~2–5% cirrus clouds [21,30]. Thus, the diurnal discrepancy is also possible to be caused by meteorological effects and should be further investigated in future studies.

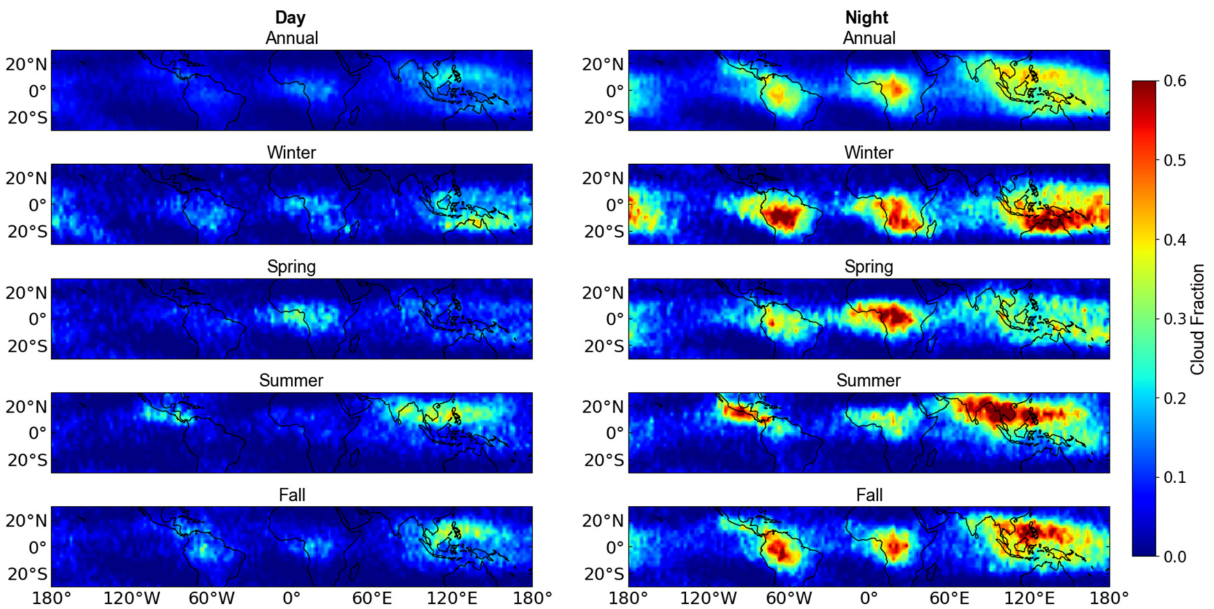

Figure 1. The spatial distribution of the tropical tropopause layer (TTL) cloud fraction with a 2.5° × 2.5° grid resolution from the joint Cloud-Aerosol Lidar and Infrared Pathfinder Satellite Observations (CALIPSO) and CloudSat observations from 2007 to 2010. Winter, spring, summer, and fall represent boreal ones, i.e., months 12–2, 3–5, 6–8, and 9–11, respectively.

TTL clouds are more frequently observed in the Western Pacific, South America, and Central Africa during both daytime and nighttime, where TTL cloud fraction can reach

~50–60% during the nighttime. The distribution characteristics of cloud fraction in Figure 1 closely resemble those of the TTL cirrus clouds as shown by Tseng and Fu [23]. In terms of the annual distribution, the highest TTL cloud fraction is found in the Western Pacific, followed by Central Africa and South America. The average cloud fraction is evidently higher in winter. The regions with frequent TTL clouds match with previous study [31], as described in Section 1.

Figure 2a,b show the monthly mean TH and tropopause temperature (TT) of the all-sky and the TTL cloud sky, respectively. Mean TTL CTH and difference of CTH−TH are displayed in Figure 2c,d. Black lines represent pixels observed under the all-sky conditions, and blue lines represent those with TTL cloud sky. Observations during the nighttime and daytime are represented by solid and dashed lines, respectively. Detailed statistics for the results are given in Table 1. Overall, TH, TT, and CTH show significant annual cycles with the coldest and highest tropopause and cloud top in boreal winter. TH varies from 15.5 to 16.8 km, TT ranges from −80 to −75 °C, and CTH is located at altitudes between 15.9 and 17.4 km.

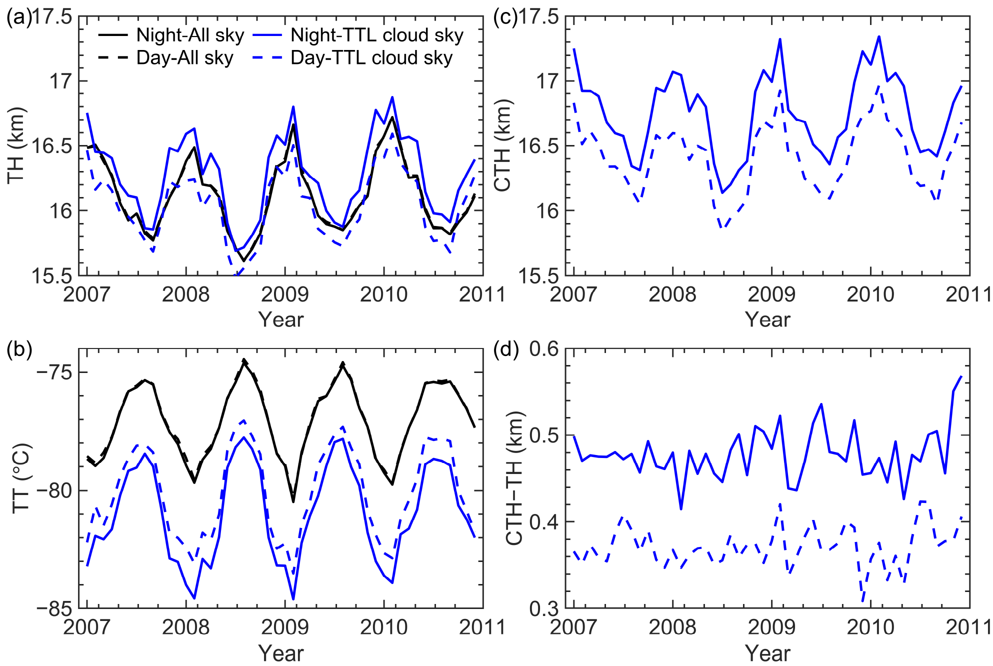

Figure 2. Time series of the monthly mean (**a**) tropopause heights (THs), (**b**) tropopause temperatures (TTs) for the all-sky (black lines) and only TTL cloud conditions (blue lines), (**c**) cloud top height (CTH), and (**d**) CTH−TH during the daytime (dashed lines) and during the nighttime (solid lines) over 30°S–30°N from joint CALIPSO and CloudSat observations from 2007 to 2010. The major tick mark for each year indicates January.

Table 1. Detailed statistics of TH, TT, CTH, and CTH−TH in TTL cloud sky and all-sky as well as during the daytime and nighttime as shown in Figure 2.

		TTL cloud sky	All-sky
Night	TH (km)	16.27	16.11
	TT (°C)	−80.97	−77.07
	CTH (km)	16.75	—
	CTH−TH (km)	0.48	—
Day	TH (km)	16.04	16.12
	TT (°C)	−80.11	−76.99
	CTH (km)	16.41	—
	CTH−TH (km)	0.37	—

Figure 2 investigates the influence of clouds on tropopause. During the daytime, the average TH over the tropics is 16.04 km, whereas the average TH over TTL cloud pixels is 16.27 km; during the daytime, the values are 16.12 and 16.04 km, respectively. It shows that TTL clouds can cause the TH to increase by about 160 m during the nighttime but decrease by about 84 m during the daytime. Furthermore, the presence of TTL clouds reduces TT from −77.07 to −80.97 °C during the nighttime by approximately 3.89 °C, and from −76.99 to −80.11 °C during the daytime by approximately 3.12 °C. It is probably because the structure of TTL clouds changes the atmospheric temperature profile, which finally manifests as that TH increases during the nighttime and decreases during the daytime in the presence of TTL clouds. The decrease in TT can be explained by the cooling effect of TTL clouds.

The diurnal differences between the tropopause and cloud top are also illustrated in Figure 2. Remarkably, the monthly average values vary according to whether data is collected during the daytime and nighttime: TH value for the night is 16.27 km and is about 230 m higher than that during the day; TTs during the nighttime and during the daytime are −80.97 and −80.11 °C, respectively, and is 0.86 °C colder during the nighttime than during the daytime. During the nighttime, CTH is about 340 m higher than that during the daytime. In addition, CTH is on average 480 m higher than TH during the nighttime, with a maximum of no more than 570 m, whereas CTH is 370 m higher than TH during the daytime.

Figure 3 illustrates the seasonal variations of the TH and TTL cloud properties averaged over four years. Compared to Figure 2, Figure 3 shows more clearly the seasonal changes and the condition of cloud tops beyond tropopause. As expected, TH, TT, and TTL CTH show significant seasonal variations. The same is seen with the result in Figure 2, the season cycle pronounces that TH and CTH are highest and TT is coldest during the boreal winter, which is originally attributed to the deeper convection within the Hadley cell and can be subsequently explained by stronger stratospheric pumping driven by stratospheric planetary waves at extratropical latitudes, which causes lower tropical cold point temperatures and deeper convection [7]. In Figure 3d, both TH and CTH over the tropics differ over 0.5 km, between 15.8 and 16.5 km or between 16.5 and 17.2 km, respectively. Due to the differences in the TH, the TT shows reasonably opposite variations with higher TH over boreal winter and colder TT over boreal summer. However, the variations for CTH−TH are not significant, representing that TTL CTH is strictly limited by the tropopause.

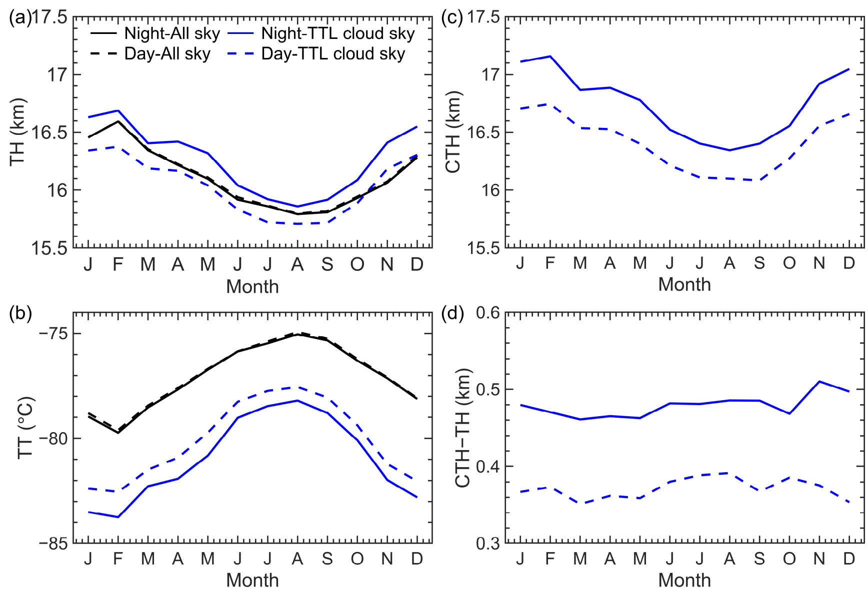

Figure 3. Same as Figure 2 but for seasonal cycles averaged over four years. Left panels are time series of the monthly mean (**a**) THs and (**b**) TTs for the all-sky (black lines) and only TTL cloud conditions (blue lines). Right panles are (**c**) CTH and (**d**) CTH−TH during the daytime (dashed lines) and during the nighttime (solid lines).

Figure 4 illustrates probability distributions of TTL CTH, CBH, and cloud CGT. The averages of CTH, CBH, and CGT are 16.65, 13.52, and 3.13 km, respectively. CTH is basically from 16 to 18 km, mainly influenced by the tropopause (Figure 4a). The probability distribution of CBH has two peak values. One is around 16 km caused by high clouds, and the other is around 1 km caused by clouds with a very deep thickness (i.e., Ns and DC). The probability distribution of CGT also has two peaks at approximately 16 km and 1 km, which is similar to that of CBH. However, clouds causing the two peaks are the opposite of that in the CBH distribution.

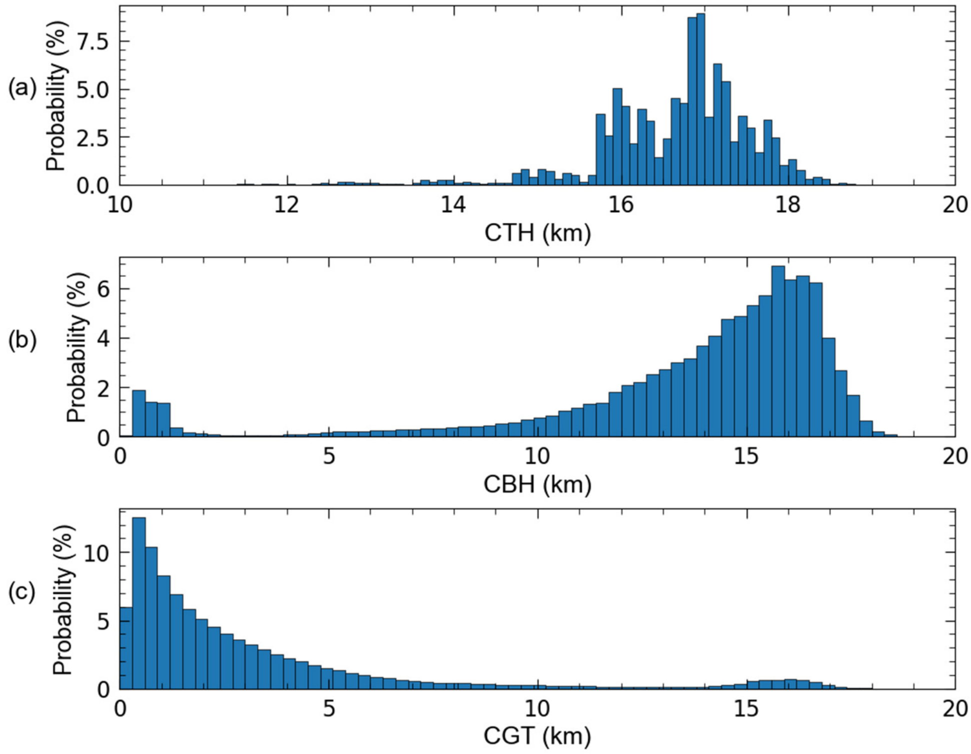

Figure 4. Probability distribution of (**a**) CTH, (**b**) cloud base height (CBH), and (**c**) cloud geometrical thickness (CGT) over 30°S–30°N from 2007 to 2010.

Figure 5 displays the proportion of profiles with different TTL cloud layer numbers to total cloud profiles. TTL clouds of 1-layer, 2-layer, and 3-layer structures account for ~30, ~40, and ~20%, respectively. Overall, ~30% of TTL clouds have a single-layer structure and the other ~70% have a multi-layer structure. Clouds with vertical structures of 2–3 layers account for about 85% of multi-layer clouds, indicating that TTL clouds generally have fewer layers. However, some pixels do detect an appreciable number of cloud layers.

Figure 6 depicts the CGTs of different cloud layers at different CTH levels and the corresponding ratios. The blue, orange, and green bars represent the single-layer TTL cloud, the uppermost layer of multi-layer clouds, and the uppermost layer of total layers, respectively. The TTL CTHs are divided into five levels: <15 km, 15–16 km, 16–17 km, 17–18 km, and >18 km. In Figure 6a, the average CGT tends to become thinner as the CTH level increases. The average CGTs are approximately 5.5, 2.1, and 3.1 km for single-layer, multi-layer, and total layers, respectively. The average CGT for multi-layer clouds is significantly thinner, which is less than half of the CGT of single-layer clouds. Figure 6b suggests that CTH is mainly distributed between 16 and 18 km (i.e., ~76%) and approximately 44% of TTL clouds have tops located between 16 and 17 km. It is consistent with the result of Figure 4a. The proportion of single-layer and multi-layer at each level is similar.

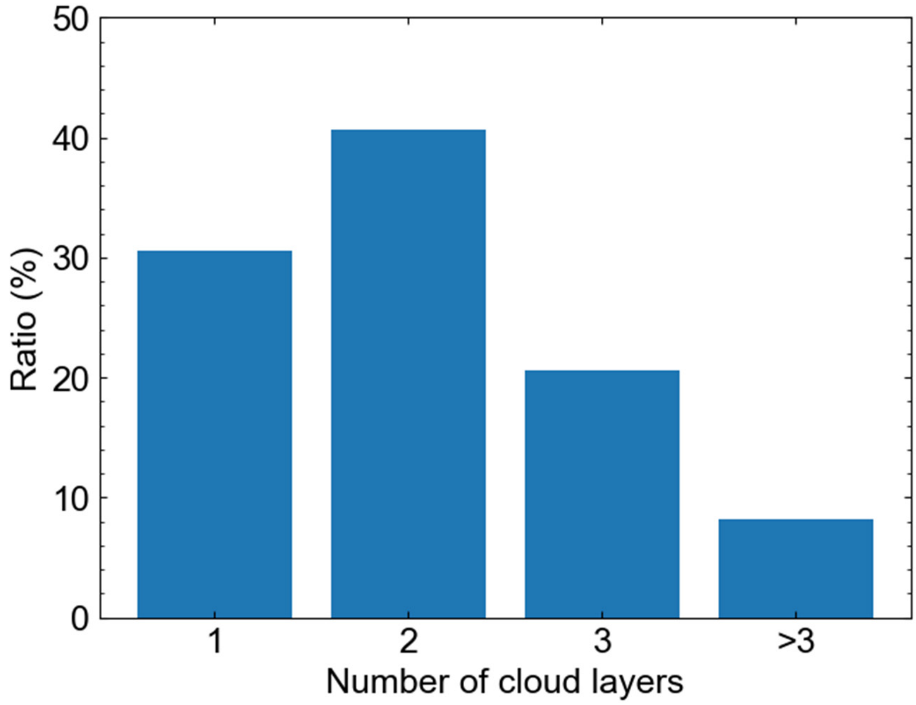

Figure 5. Ratios of profiles with different cloud layer numbers to total cloud profiles over 30°S–30°N from 2007 to 2010.

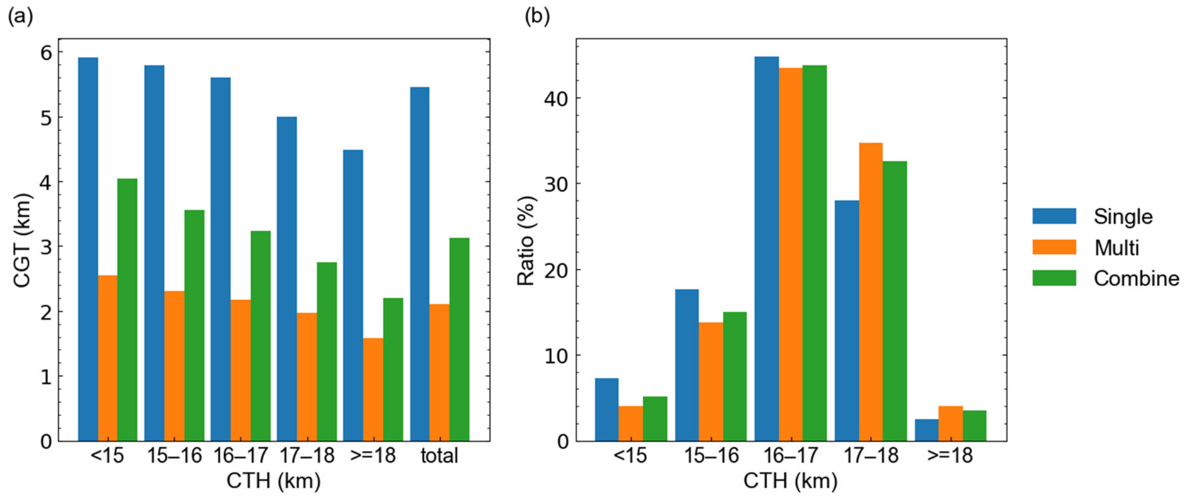

Figure 6. (**a**) Mean CGT and (**b**) ratios for single-layer (blue), the uppermost layer of multi-layer (orange), and total layers (green) of CTH < 15 km, 15–16 km, 16–17 km, 17–18 km, and >=18 km, respectively. Attached with the total average of CGT in the left panel.

Figure 7 illustrates the ratio and partially enlarged ratio of different types of single-layer clouds, multi-layer clouds, and total layers. Clouds are divided into five types (high cloud, As, Ns, DC, and other types) based on the eight categories of the 2B-CLDCLASS-LIDAR product, and high cloud consists of cirrus and cirrostratus cloud though they could not be further classified in the dataset. As described in Section 2, As, Ns, and DC represent altostratus, nimbostratus, and deep convective clouds, and the other cloud type includes Ac, St, Sc, and Cu. Figure 7 shows that TTL clouds are predominately composed of high clouds (cirrus and cirrostratus) with an average ratio of ~91% and ~4.8% of TTL clouds are Ns and DC overall. For single-layer TTL clouds, high clouds and As occupy ~75% and ~9%, respectively, and the ratios of Ns and DC are approximately 15.5%. For multi-layer TTL clouds, high clouds take up ~98%. Figure 7 indicates that convection-associated clouds, i.e., Ns and DC, tend to be a single-layer structure.

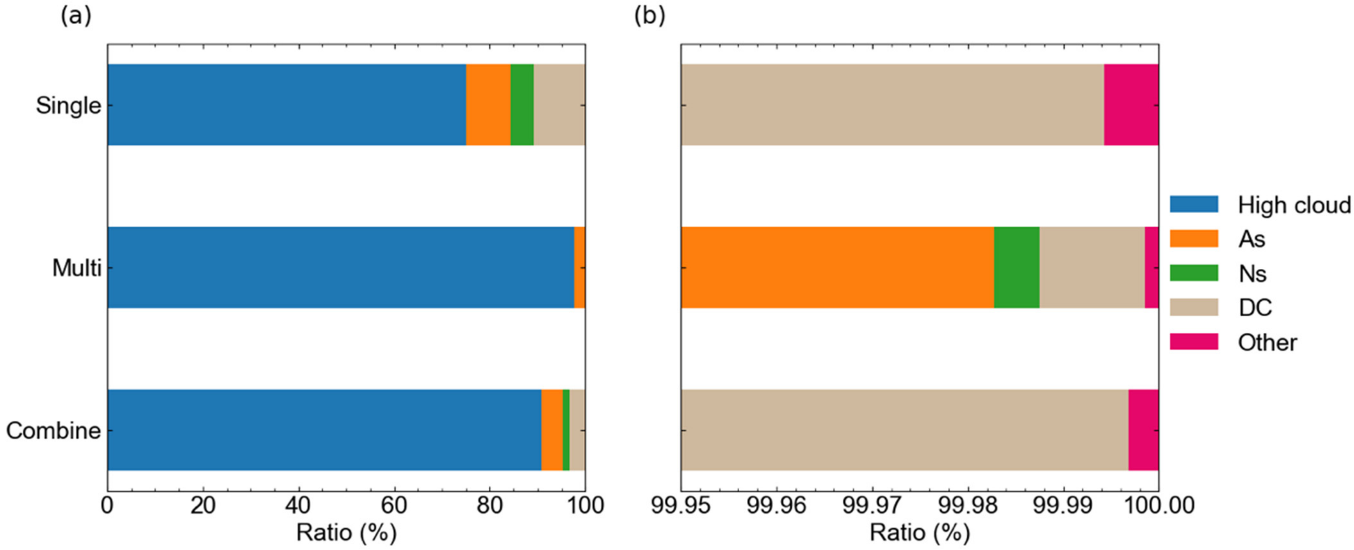

Figure 7. (**a**) Ratios and (**b**) enlarged ratio picture from 99.95 to 100% of cloud types for single layer, the uppermost layer of multi-layer, and their combination. As, Ns and DC represent altostratus, nimbostratus, and deep convective clouds. The other cloud type includes Ac (altocumulus), St (stratus), Sc (stratocumulus), and Cu (cumulus).

We count the pixel numbers and the corresponding percentage of the cloud phase for single-layer, multi-layer, and total layers (not shown here). Over 4 million pixels are collected in this study, of which ~30% are single-layer clouds while the remaining 70% are multi-layer clouds. Overall, TTL clouds are in a predominate ice phase with a ratio of ~94% and a small water phase with ~6% percentage. For single-layer clouds, ~81% of TTL clouds are with the ice phase and ~19% of TTL clouds are with the water phase, while almost all TTL clouds are with the ice phase for multi-layer clouds. The result is consistent with that of the cloud type in Figure 7. The water phase of single-layer TTL clouds is mainly from Ns and DC and partly from As.

4. Discussion

As presented in Section 3, we discuss the diurnal and seasonal differences in the spatial distributions of TTL clouds. To reveal the influence of clouds on the tropopause, we further compare the time series and seasonal cycles of tropopause in the presence of TTL cloud sky and all-sky condition and investigate the diurnal differences between the tropopause and cloud top. The probability distributions of CTH, CBH, CGT, and cloud layer numbers are studied as well. Based on the number of cloud layers, clouds are divided into single-layer, multi-layer, and total layers. The corresponding CGT and the ratio at different CTHs are studied, as well as cloud categories and phases.

The influence of clouds on tropopause and the diurnal differences between tropopause and cloud top are presented in Figures 2 and 3. Generally, the existence of TTL clouds can cool TT by ~3.5 °C both during the daytime and nighttime, which can be explained by the release of condensation heat in the TTL cloud formation. The cold surrounding in the TTL is called "cold trap" [32] and is common in the Western Pacific during the boreal winter. Our results show that the average TH with TTL clouds is ~160 m higher than that with the all-sky cases during the nighttime, and Fu et al. [24] and Ali et al. [33] indicated that the TTL clouds may lift TH due to their radiative effects. However, the differences on TH for TTL cloud and all-sky cases during the daytime are less noticeable, and such discrepancy should be investigated by further comparison of cloud radiation effects as well as other factors during the daytime and nighttime.

Generally, the accuracy of TH based on either reanalysis data or model assimilation is with small errors, i.e., typically less than ±150 m [34]. To be more specific, the uncertainty of GOES-5 TH we used is approximately 140 m (average differences) according to the study of Pan and Munchak [35] by comparing with radiosonde measurements. Another important source of uncertainties in our TTL cloud study is those related to the observations, which can be caused by many factors, e.g., the vertical sampling grid size (see Section 2), the magnitude of signal-to-noise, the interference of stratospheric aerosols with clouds, and so on. For the signal-to-noise magnitude, the detection sensitivity of CALIOP measurements averaged over 5 km during the daytime is around 1.5 orders of magnitude lower than during the nighttime [36]; therefore, CALIOP daytime data may miss roughly 5% of clouds due to reduced lidar sensitivity during the daytime [30].

Using four years of observations, we quantified and analyzed TTL cloud properties. This analysis is important for understanding TTL clouds and the effects of clouds on the tropopause in TTL. We focus on the diurnal discrepancy of TTL clouds, which were less reported, and also notice that the impacts, i.e., lifting or lowering, of cloud presence on TH during the nighttime and daytime was opposite, and more efforts should be made to further quantify and understand such differences in future studies.

5. Conclusions

This study quantifies and analyzes TTL cloud properties based on CALIPSO and CloudSat joint measurements from 2007 to 2010. More reliable tropopause information based on the GOES-5 reanalysis dataset is considered to extract TTL clouds. TTL clouds are defined as cloudy pixels with CTH above the TH. TTL cloud pixels we used are within the uppermost cloud layer in each profile identified by the joint CloudSat–CALIPSO classification algorithm. During the four years, the combined product gives a total of approximately 50 million pixels within the tropics, and ~4.5 million are TTL cloudy pixels. Thus, the cloud classification, CTH, CBH, and phase information are summarized.

It is shown that TTL cloud occurrence frequency during the daytime is half of that during the nighttime due to significant missing of cirrus cloud detection during the daytime. The average TH, TT, and CTH are 16.2 km, −80.7 °C, and 16.6 km, respectively, and the cloud top average exceeds tropopause by approximately 500 m. The presence of TTL clouds causes a corresponding change in TH and TT, with an average decrease of 3–4 °C in TT, an increase of 160 m in TH during the nighttime, and a decrease of 84 m in TH during the daytime. The diurnal differences between the tropopause and cloud top indicate that tropopause is higher (i.e., 230 m of TH and 340 m of CTH) and colder (~0.86 °C) during the nighttime. Among the 30% single-layer clouds, ~15% are convection-related clouds, ~75% are high clouds, while multi-layer clouds are ~98% high clouds. However, this study considered all TTL clouds together, and we will further investigate their regional differences, e.g., differences between TTL clouds over ocean and land, in the future. Furthermore, the radiative effects of TTL clouds of different kinds would also be discussed.

Author Contributions: Conceptualization, B.Y., S.L. and S.T.; data curation, S.L.; formal analysis, S.L., X.Z., Y.L. and B.Y.; funding acquisition, B.Y. and S.L.; methodology, B.Y., S.L., Y.L. and X.Z.; software, S.L.; visualization, S.L. and Y.L.; writing—original draft preparation, S.L., X.Z., Y.L. and S.T.; writing—review and editing, S.L., X.Z., Y.L., S.T. and B.Y. All authors have read and agreed to the published version of the manuscript.

Funding: This research was funded by the National Natural Science Foundation of China (Grant 42122038), the Postgraduate Research and Practice Innovation Program of Jiangsu Province (Grant KYCX22_1169) and Defense Industrial Technology Development Program.

Institutional Review Board Statement: Not applicable.

Informed Consent Statement: Not applicable.

Data Availability Statement: All data in this work are publicly available online for all researchers. The CALIOP version 4.20 cloud profile product (05kmCPro) is available from https://subset.larc.nasa.

gov/calipso/login.php (accessed on 21 February 2022). The joint CloudSat and CALIPSO version P1_R05 cloud classification product (2B-FLXHR-LIDAR) is downloaded at https://www.icare.univ-lille.fr/ (accessed on 21 February 2022) from the ICARE Data and Services Center.

Acknowledgments: We thank NASA Langley Research Center Atmospheric Sciences Data Center for freely providing their high-quality CALIPSO data. We thank ICARE Data and Services Center for providing access to the joint CloudSat and CALIPSO data used in this study. The simulations are conducted in the High-Performance Computing Center of Nanjing University of Information Science & Technology.

Conflicts of Interest: The authors declare no conflict of interest.

References

1. Fueglistaler, S.; Dessler, A.E.; Dunkerton, T.J.; Folkins, I.; Fu, Q.; Mote, P.W. Tropical Tropopause Layer. *Rev. Geophys.* **2009**, *47*, RG1004. [CrossRef]
2. Randel, W.J.; Jensen, E.J. Physical Processes in the Tropical Tropopause Layer and Their Roles in a Changing Climate. *Nat. Geosci.* **2013**, *6*, 169–176. [CrossRef]
3. Dessler, A.E.; Schoeberl, M.R.; Wang, T.; Davis, S.M.; Rosenlof, K.H. Stratospheric Water Vapor Feedback. *Proc. Natl. Acad. Sci. USA* **2013**, *110*, 18087–18091. [CrossRef]
4. Tegtmeier, S.; Anstey, J.; Davis, S.; Dragani, R.; Harada, Y.; Ivanciu, I.; Pilch Kedzierski, R.; Krüger, K.; Legras, B.; Long, C.; et al. Temperature and Tropopause Characteristics from Reanalyses Data in the Tropical Tropopause Layer. *Atmos. Chem. Phys.* **2020**, *20*, 753–770. [CrossRef]
5. Corti, T.; Luo, B.P.; Fu, Q.; Vömel, H.; Peter, T. The Impact of Cirrus Clouds on Tropical Troposphere-to-Stratosphere Transport. *Atmos. Chem. Phys.* **2006**, *6*, 2539–2547. [CrossRef]
6. Haladay, T.; Stephens, G. Characteristics of Tropical Thin Cirrus Clouds Deduced from Joint CloudSat and CALIPSO Observations. *J. Geophys. Res.* **2009**, *114*, D00A25. [CrossRef]
7. Virts, K.S.; Wallace, J.M. Annual, Interannual, and Intraseasonal Variability of Tropical Tropopause Transition Layer Cirrus. *J. Atmos. Sci.* **2010**, *67*, 3097–3112. [CrossRef]
8. Ali, S.; Mehta, S.K.; Ananthavel, A.; Reddy, T.V.R. Temporal and Vertical Distributions of the Occurrence of Cirrus Clouds over a Coastal Station in the Indian Monsoon Region. *Atmos. Chem. Phys.* **2022**, *22*, 8321–8342. [CrossRef]
9. Woods, S.; Lawson, R.P.; Jensen, E.; Bui, T.P.; Thornberry, T.; Rollins, A.; Pfister, L.; Avery, M. Microphysical Properties of Tropical Tropopause Layer Cirrus. *J. Geophys. Res. Atmos.* **2018**, *123*, 6053–6069. [CrossRef]
10. Peter, T.; Luo, B.P.; Wirth, M.; Kiemle, C.; Flentje, H.; Yushkov, V.A.; Khattatov, V.; Rudakov, V.; Thomas, A.; Borrmann, S.; et al. Ultrathin Tropical Tropopause Clouds (UTTCs): I. Cloud Morphology and Occurrence. *Atmos. Chem. Phys.* **2003**, *3*, 1083–1091. [CrossRef]
11. Lawson, R.P.; Pilson, B.; Baker, B.; Mo, Q.; Jensen, E.; Pfister, L.; Bui, P. Aircraft Measurements of Microphysical Properties of Subvisible Cirrus in the Tropical Tropopause Layer. *Atmos. Chem. Phys.* **2008**, *8*, 1609–1620. [CrossRef]
12. Gettelman, A.; Salby, M.L.; Sassi, F. Distribution and Influence of Convection in the Tropical Tropopause Region. *J. Geophys. Res. Atmos.* **2002**, *107*, ACL 6-1–ACL 6-12. [CrossRef]
13. Liu, C.; Zipser, E.J. Global Distribution of Convection Penetrating the Tropical Tropopause. *J. Geophys. Res.* **2005**, *110*, D23104. [CrossRef]
14. Ueyama, R.; Jensen, E.J.; Pfister, L.; Diskin, G.S.; Bui, T.P.; Dean-Day, J.M. Dehydration in the Tropical Tropopause Layer: A Case Study for Model Evaluation Using Aircraft Observations. *J. Geophys. Res. Atmos.* **2014**, *119*, 5299–5316. [CrossRef]
15. Frey, W.; Borrmann, S.; Fierli, F.; Weigel, R.; Mitev, V.; Matthey, R.; Ravegnani, F.; Sitnikov, N.M.; Ulanovsky, A.; Cairo, F. Tropical Deep Convective Life Cycle: Cb-Anvil Cloud Microphysics from High-Altitude Aircraft Observations. *Atmos. Chem. Phys.* **2014**, *14*, 13223–13240. [CrossRef]
16. Pandit, A.K.; Gadhavi, H.; Ratnam, M.V.; Jayaraman, A.; Raghunath, K.; Rao, S.V.B. Characteristics of Cirrus Clouds and Tropical Tropopause Layer: Seasonal Variation and Long-Term Trends. *J. Atmos. Sol. Terr. Phys.* **2014**, *121*, 248–256. [CrossRef]
17. Hollars, S.; Fu, Q.; Comstock, J.; Ackerman, T. Comparison of Cloud-Top Height Retrievals from Ground-Based 35 GHz MMCR and GMS-5 Satellite Observations at ARM TWP Manus Site. *Atmos. Res.* **2004**, *72*, 169–186. [CrossRef]
18. Liu, C.; Song, Y.; Zhou, G.; Teng, S.; Li, B.; Xu, N.; Lu, F.; Zhang, P. A cloud optical and microphysical property product for the advanced geosynchronous radiation imager onboard China's Fengyun-4 satellites: The first version. *Atmos. Ocean. Sci. Lett.* **2023**, 100337. [CrossRef]
19. Sherwood, S.C.; Chae, J.-H.; Minnis, P.; McGill, M. Underestimation of Deep Convective Cloud Tops by Thermal Imagery. *Geophys. Res. Lett.* **2004**, *31*, L11102. [CrossRef]
20. Stephens, G.L.; Vane, D.G.; Boain, R.J.; Mace, G.G.; Sassen, K.; Wang, Z.; Illingworth, A.J.; O'Connor, E.J.; Rossow, W.B.; Durden, S.L.; et al. The Cloudsat Mission and the A-Train: A New Dimension of Space-Based Observations of Clouds and Precipitation. *Bull. Am. Meteorol. Soc.* **2002**, *83*, 1771–1790. [CrossRef]
21. Sassen, K.; Wang, Z.; Liu, D. Cirrus Clouds and Deep Convection in the Tropics: Insights from CALIPSO and CloudSat. *J. Geophys. Res.* **2009**, *114*, D00H06. [CrossRef]

22. Feng, J.; Huang, Y. Impacts of Tropical Cyclones on the Thermodynamic Conditions in the Tropical Tropopause Layer Observed by A-Train Satellites. *Atmos. Chem. Phys.* **2021**, *21*, 15493–15518. [CrossRef]
23. Tseng, H.-H.; Fu, Q. Tropical Tropopause Layer Cirrus and Its Relation to Tropopause. *J. Quant. Spectrosc. Radiat. Transf.* **2017**, *188*, 118–131. [CrossRef]
24. Fu, Q.; Smith, M.; Yang, Q. The Impact of Cloud Radiative Effects on the Tropical Tropopause Layer Temperatures. *Atmosphere* **2018**, *9*, 377. [CrossRef]
25. Winker, D.M.; Pelon, J.; Coakley, J.A.; Ackerman, S.A.; Charlson, R.J.; Colarco, P.R.; Flamant, P.; Fu, Q.; Hoff, R.M.; Kittaka, C.; et al. The CALIPSO Mission: A Global 3D View of Aerosols and Clouds. *Bull. Am. Meteorol. Soc.* **2010**, *91*, 1211–1230. [CrossRef]
26. Rienecker, M. *File Specification for GEOS-5 DAS Gridded Output*; NASA Goddard Space Flight Center: Greenbelt, MD, USA, 2008. Available online: https://gmao.gsfc.nasa.gov/GMAO_products/documents/GEOS-5.2.0_File_Specification.pdf (accessed on 2 January 2023).
27. Winker, D. Data Quality Summary for the CALIPSO Version 4.20 and V4.21 Lidar Level 2 Data Products. Available online: https://www-calipso.larc.nasa.gov/resources/calipso_users_guide/qs/cal_lid_l2_all_v4-20.php (accessed on 3 January 2023).
28. Sassen, K.; Wang, Z.; Liu, D. Global Distribution of Cirrus Clouds from CloudSat/Cloud-Aerosol Lidar and Infrared Pathfinder Satellite Observations (CALIPSO) Measurements. *J. Geophys. Res.* **2008**, *113*, D00A12. [CrossRef]
29. Pauly, R.M.; Yorks, J.E.; Hlavka, D.L.; McGill, M.J.; Amiridis, V.; Palm, S.P.; Rodier, S.D.; Vaughan, M.A.; Selmer, P.A.; Kupchock, A.W.; et al. Cloud-Aerosol Transport System (CATS) 1064 nm Calibration and Validation. *Atmos. Meas. Tech.* **2019**, *12*, 6241–6258. [CrossRef]
30. Noel, V.; Chepfer, H.; Chiriaco, M.; Yorks, J. The Diurnal Cycle of Cloud Profiles over Land and Ocean between 51° S and 51° N, Seen by the CATS Spaceborne Lidar from the International Space Station. *Atmos. Chem. Phys.* **2018**, *18*, 9457–9473. [CrossRef]
31. Paulik, L.C.; Birner, T. Quantifying the Deep Convective Temperature Signal within the Tropical Tropopause Layer (TTL). *Atmos. Chem. Phys.* **2012**, *12*, 12183–12195. [CrossRef]
32. Holton, J.R.; Gettelman, A. Horizontal Transport and the Dehydration of the Stratosphere. *Geophys. Res. Lett.* **2001**, *28*, 2799–2802. [CrossRef]
33. Ali, S.; Mehta, S.K.; Annamalai, V.; Ananthavel, A.; Reddy, R. Qualitative Observations of the Cirrus Clouds Effect on the Thermal Structure of the Tropical Tropopause. *J. Atmos. Sol. Terr. Phys.* **2020**, *211*, 105440. [CrossRef]
34. Xian, T.; Homeyer, C.R. Global Tropopause Altitudes in Radiosondes and Reanalyses. *Atmos. Chem. Phys.* **2019**, *19*, 5661–5678. [CrossRef]
35. Pan, L.L.; Munchak, L.A. Relationship of Cloud Top to the Tropopause and Jet Structure from CALIPSO Data. *J. Geophys. Res. Atmos.* **2011**, *116*, D12201. [CrossRef]
36. Yorks, J.E.; McGill, M.J.; Palm, S.P.; Hlavka, D.L.; Selmer, P.A.; Nowottnick, E.P.; Vaughan, M.A.; Rodier, S.D.; Hart, W.D. An Overview of the CATS Level 1 Processing Algorithms and Data Products. *Geophys. Res. Lett.* **2016**, *43*, 4632–4639. [CrossRef]